Advanced Powder Technology 23 (2012) 315–323

Contents lists available at ScienceDirect

Advanced Powder Technology

journal homepage: www.elsevier.com/locate/apt

Original Research Paper

Magnetic and catalytic properties of cubic copper ferrite nanopowders synthesized from secondary resources

M.M. Rashad [a,*], R.M. Mohamed [a,b,c], M.A. Ibrahim [a], L.F.M. Ismail [d], E.A. Abdel-Aal [a]

[a] Advanced materials department, Central Metallurgical R&D Institute, CMRDI, P.O. Box 87 Helwan, Cairo, Egypt
[b] Chemistry Department, Faculty of Science, King Abdulaziz University, P.O. Box : 80203 Jeddah: Saudi Arabia
[c] Center of Excellence in Environmental Studies, King Abdulaziz University, P.O Box: 80216 Jeddah 21589, Saudi Arabia
[d] Chemistry Department, Faculty of Science, Al-Azhar Universty, Cairo, Egypt

ARTICLE INFO

Article history:
Received 23 January 2011
Received in revised form 5 April 2011
Accepted 6 April 2011
Available online 20 April 2011

Keywords:
Industrial wastes
Ferrites
Nanomaterials
Magnetic properties
Photocatalytic properties

ABSTRACT

Cubic copper ferrite $CuFe_2O_4$ nanopowders have been synthesized via a hydrothermal route using industrial wastes. The synthesis conditions were systematically studied using statistical design (Box–Behnken Program) and the optimum conditions were determined. The results revealed that single phase of cubic copper ferrite powders can be obtained at different temperatures from 100 to 200 °C for times from 12 to 36 h with pH values 8–12. The crystallite size of the produced powders was in the range between 24.6 and 51.5 nm. The produced copper ferrite powders were appeared as a homogeneous pseudo-cubic-like structure. A high saturation magnetization (M_s 83.7 emu/g) was achieved at hydrothermal temperature 200 °C for 24 h and pH 8. Photocatalytic degradation of the methylene blue dye using copper ferrite powders produced at different conditions was investigated. A good catalytic efficiency was 95.9% at hydrothermal temperature 200 °C for hydrothermal time 24 h at pH 12 due to high surface area (118.4 m^2/g).

1. Introduction

Copper ferrite ($CuFe_2O_4$) is one of the important spinel ferrites MFe_2O_4 because it exhibits phase transitions, changes semiconducting properties, shows electrical switching and tetragonality variation when treated under different conditions in addition to interesting magnetic and electrical properties with chemical and thermal stabilities [1]. It is used in the wide range of applications in gas sensing [2], catalytic applications [3–5], Li ion batteries [6] high density magneto-optic recording devices, color imaging, bioprocessing, magnetic refrigeration and ferrofluids [1,7]. Moreover, $CuFe_2O_4$ assumes great significance because of its high electric conductivity, high thermal stability and high catalytic activity for O_2 evolution from alumina–cryolite system used for aluminum production [8].

$CuFe_2O_4$ is known to exist in tetragonal and cubic structures. Under slow cooling Cu-ferrite crystallizes in a tetragonal structure with lattice parameter ratio c/a of about 1.06. Tetragonal phase of Cu-ferrite has inverse spinel structure with almost all Cu^{2+} ions occupying octahedral sublattice, whereas Fe^{3+} ions divide equally between the tetrahedral and octahedral sublattices [9]. The tetragonal structure is stable at room temperature and transforms to cubic phase only at a temperature of 360 °C and above due to Jahn–Teller distortion. The distortion is directly related to the magnetic properties. The cubic structure possesses a larger magnetic moment than that of the tetragonal one, because there are more cupric ions (Cu^{2+}) at tetrahedral sites in cubic structure as compared to that in the case of tetragonal structure [10]. Nano-sized copper spinel ferrites show unusual properties in comparison with their bulk analogs and receive enormous attention during last decade because of their potential applications. They can be obtained by variety of methods such as solid state reaction [11], mechanochemical [12], sol–gel [13], co-precipitation [14], and combustion synthesis [15], polyol route [16] and microemulsion-hydrothermal route [17]. Most of the previous route led to the formation of tetragonal copper ferrite. From the best of our knowledge, a rarely reported mentioned the synthesis of cubic copper ferrite powders via the hydrothermal route. The correlation between the magnetic and catalytic properties and the microstructure of the produced cubic copper ferrite via the hydrothermal technique need intensive work.

Due to the potential applications of ferrites, recently, special attention is focused to synthesis ferrites from industrial wastes. Copper ferrite $CuFe_2O_4$ is prepared from copper sludge which collected from a filter press of waste-water treatment process in a surface finishing plant with analytical grade iron oxide powder using ball milling technique [18]. Nano-sized magnetic particles are synthesized from spent pickling liquors by ultrasonic-assisted chemical co-precipitation [19]. Furthermore, $Zn_xFe_{3-x}O_4$, $Ni_xFe_{3-x}O_4$

* Corresponding author. Tel./fax: +20 2 25010639.
E-mail address: rashad133@yahoo.com (M.M. Rashad).

0921-8831/$ - see front matter © 2011 The Society of Powder Technology Japan. Published by Elsevier B.V. and The Society of Powder Technology Japan. All rights reserved.
doi:10.1016/j.apt.2011.04.005

and $Cr_xFe_{3-x}O_4$ ($0 < x < 1$) were synthesized using wet method [20]. In addition, magnetite Fe_3O_4 particles [21] and Mn–Zn ferrite magnetic materials [22] have been synthesized from the waste water and recycling spent zinc manganese dioxide batteries. Moreover, Rashad et al. synthesized $CuFe_2O_4$ from the mill scale, waste of steel industry through solid state [23] $Cu_{0.5}Zn_{0.5}Fe_2O_4$ using Cu–Zn spent catalyst consumed in fertilizer industries with ferrous sulfate from the etching during steel industries [24], and $NiFe_2O_4$ [25] using fly ash, respectively.

Statistical experimental designs have been used for several decades and they can be adopted at various phases of an optimization strategy, such as for screening experiments or for looking for the optimal conditions of targeted responses [26]. Applying the Box–Behnken design is an efficient method to optimize the selected factors as well as to test the effect of factors interaction. Besides it converted the materials synthesis factors correlations into a mathematical model that predicted where the optimal is likely to be located. It is worthwhile to advise the materials industries sponsors to apply such experimental design to maintain high efficiency and profit process. In our previous work, Rashad et al. used the Box–Behnken design model to optimize the synthesis conditions of Ni [27], $BaTiO_3$ [28], $MgSnO_3$ [26], YIG [29] and silica nanosphere [30]. Moreover, other published papers in the literature have been done to apply this design for optimizing operation of an integrated membrane system (IMS) [31], food control [32] biochemistry and pharmaceutics [26]. Therefore, in the present work, the produced copper wastes during printed circuit boards industry and ferric sulfate wastes from the etching during iron and steel making, which highly exceed the levels permissible by environmental laws for dumping into sewage systems were treated with sulfuric acid to form sulfates solutions which is precipitated at pH 8–12 using 5 M NaOH solution. Box–Behnken design was applied to optimize the synthesis of copper ferrites powders via the hydrothermal method and to develop a relationship between magnetic properties of the produced powder and the three synthesis variables (hydrothermal temperature, time and pH value). In addition, effect of the variables on $CuFe_2O_4$ phase formation, crystallite size, microstructure and photocatalytic properties towards methylene blue were studied.

2. Experimental

2.1. Materials

In the finishing of steel prior to plating or coating at iron and steel company, Helwan, Egypt, the steel sheet or rod is passed through pickling baths of sulfuric acid. This treatment produces large quantities of iron(II) sulfate as a by-product.

$$Fe + H_2SO_4 \rightarrow FeSO_4 + H_2$$

The produced ferrous sulfate does not contain metals but contains free sulfuric acid ~10%, 0.01 Zn^{2+} and 2% silica which were removed with dissolution with deionized water.

Cu waste was supplied by Banha for the Electronic Industries, Egypt. It was produced from spent copper etchant solutions resulting from the printed circuit boards industry then neutralized with sodium hydroxide. The waste contained 12.5% Cu, 8.7% Cl^- with minor Ni 0.001%.

2.2. Procedure

Copper ferrite powders were synthesized as the following: Cu-waste from etching of the integrated circuits boards during the electronic industries was treated with 1 M concentrated sulfuric acid (50%) at 60 °C for 15 min. The formed copper sulfate solution was mixed with stoichiometric amount of ferrous sulfate waste from iron and steel making (Fe:Cu mole ratio 2:1) according to the following equation:

$$Cu^{2+} + 2Fe^{2+} + 4O^{2-} \rightarrow CuFe_2O_4 \quad (1)$$

Then a certain volume of 5 M NaOH was added to the solution until brownish black precipitate precursor $Cu(OH)_2{\cdot}2Fe(OH)_2$ was formed instantaneously. The precipitate was filtered, washed by deionized water, and then dried at 100 °C overnight. In this work, effects of three main variables for the preparation of $CuFe_2O_4$ via hydrothermal method; hydrothermal temperature (100–200 °C), calcination time (12–36 h) and pH (8–12) on the crystal structure, crystallite size, morphology, and the magnetic properties of the produced $CuFe_2O_4$ powder were studied. The optimum conditions of copper ferrite were obtained. The design-matrix of different runs, 15 experiments, as well as the levels of each factor are shown in Table 1.

Plots of the response surface, contours, and the best predictive models for the estimate of the response variable were developed. The Box–Behnken design in Table 1 can fit the following model [20]:

$$E(y) = \beta_0 + \sum_{i=1}^{3}\beta_i x_i + \sum_{i=1}^{3}\sum_{j=1}^{3}\beta_{ij}x_i x_j + \sum_{i=1}^{3}\beta_{ii}x_i^2 \quad (2)$$

where $E(y)$ is sum of the response variable and y estimate of the response variable (crystallite size, Magnetic parameters "M_s, M_r, and H_c") and Xi's are the independent variables (pH, time and temperature) that are known for each experimental run. The parameter β_o is model constant, β_i is liner coefficients, β_{ii} is the quadratic coefficients and β_{ij} is the cross-product coefficients. The quality of fit of the polynomial model equation was expressed by the coefficient of determination R^2. Software package, Design Expert 6.1, Stat-Ease, Inc., Minneapolis, USA, was used for regression analysis of experimental data and to plot response surface. Analysis of variance (ANOVA) was used to estimate the statistical parameters. The extent of fitting the experimental results to the polynomial model equation was expressed by the determination coefficient R^2. *F*-Test was used to estimate the significant of all terms in the polynomial equation within 95% confidence interval. Experiments were performed in triplicate and mean value were given.

Table 1
Box–Behnken design with the 3 levels and 3 variables.

Run No.	Coded factor level		
	Temperature (°C)	Time (h)	pH
R1	−1	−1	0
R2	+1	−1	0
R3	−1	+1	0
R4	+1	+1	0
R5	−1	0	−1
R6	+1	0	−1
R7	−1	0	+1
R8	+1	0	+1
R9	0	−1	−1
R10	0	+1	−1
R11	0	−1	+1
R12	0	+1	+1
R13	0	0	0
R14	0	0	0
R15	0	0	0
Factors and levels for experimental design using Box–Behnken method			
Variable	−1	0	+1
Temperature (°C)	100	150	200
Time (h)	12	24	36
pH	8	10	12

2.3. Physical characterization

The final products were characterized using X-ray diffraction (XRD) on a Bruker axis D8 using Cu Kα radiation (λ = 1.540 Å). The average crystallite size of the powders was estimated automatically from corresponding XRD data using Scherrer formula. SEM images of the nanocrystalline powders were taken with a Scanning Electron Microscopy (SEM, JEOL Model 6300 F). The magnetic properties of the ferrites were measured at room temperature using a VSM (9600-1 LDJ, USA) in a maximum applied field of 16 kOe. From the obtained hysteresis loops, the saturation magnetization M_S, remanence magnetization M_r and coercivity H_c were determined. Specific surface area (S_{BET}) of samples was determined by BET surface area analyzer (Nova 2000 series, Quantachrome Instruments, UK).

Photocatalytic activity of the copper ferrite particles was evaluated by measuring the photocatalytic degradation of methylene blue ((MB, $C_{16}H_{18}ClN_3S$) in water under the illumination of UV light (high pressure mercury vapor lamp, 150 W, predominantly wavelength 254 nm) using UV/Vis/NIR spectrophotometer (V-570, JASCO, Japan). The methylene blue concentration employed was 100 ppm with 0.1 g $CuFe_2O_4$ then transferred to the cell used for irradiation experiments. The cells were exposed to the UV lamp (150 W) for 60 min at room temperature. The major absorption band of methylene blue was around 665 nm. In order to investigate the photocatalytic activities of $CuFe_2O_4$, the mineralization of methylene blue was evaluated according to the absorption change spectrophotometer (at 665 nm) in liquid cuvette configuration with de-ionized water as reference. The photocatalytic degradation efficiency of methylene blue dye was calculated by applying the following equation:

$$\text{Degradation } \% = [C_0 - C)/C_0]100 \quad (3)$$

where, C_0 is the initial dye concentration and C is the dye concentration after degradation by the copper ferrite catalyst.

3. Results and discussion

Figs. 1 and 2 show the XRD patterns of the copper waste and ferrous sulfate from etching of the integrated circuits board during manufacture of the electronic devices industries and the etching in

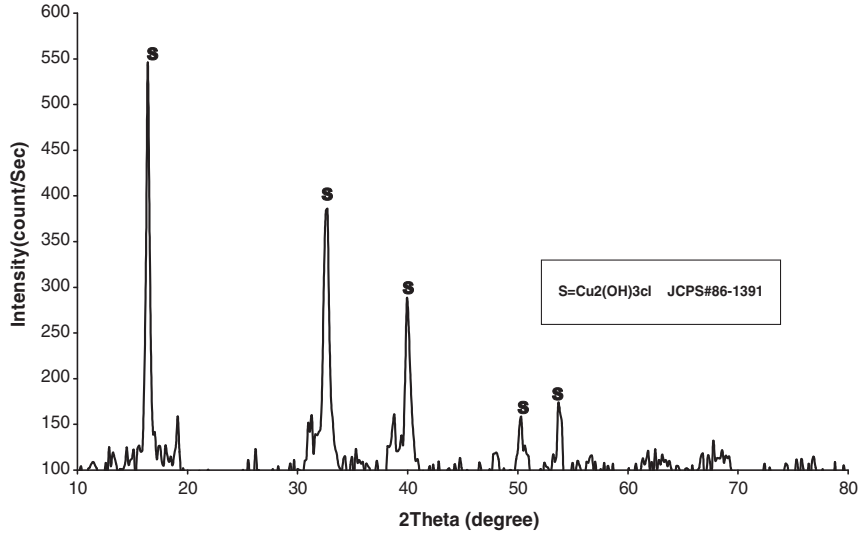

Fig. 1. XRD patterns of the copper waste produced from the etching solution of integrated circuits boards of the electronic devices industry.

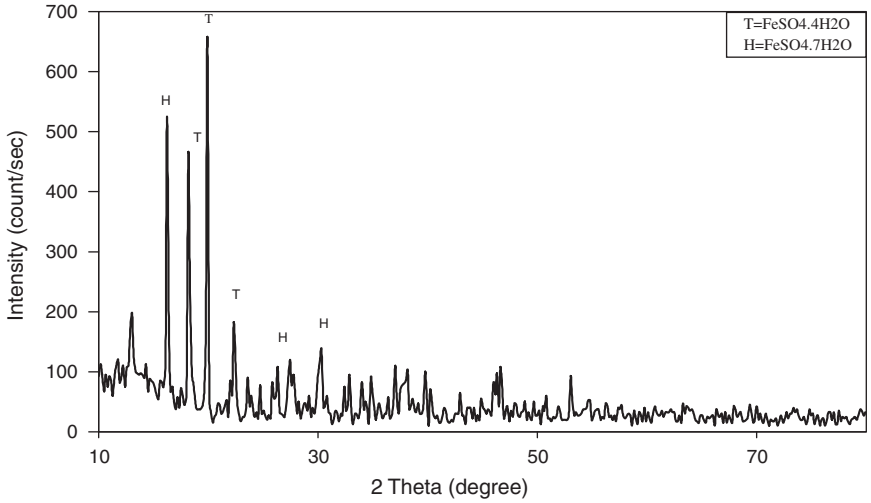

Fig. 2. XRD pattern of ferrous sulfate waste from the etching during steel making industry.

the iron and steel making, respectively. The results revealed that the copper waste is clinoatacamite, copper trihydroxy chloride salt $Cu_2(OH)_3Cl$ phase. However, the iron waste contained ferrous sulfate tetrahydrate $FeSO_4{\cdot}4H_2O$ as the main phase with ferrous sulfate heptahydrate as the secondary phase $FeSO_4{\cdot}7H_2O$. The chemical analysis of two wastes using atomic absorption spectroscopy showed that the Cu and Fe ratios were 12.5% and 18.5%, respectively.

The copper ferrite powders were formed by transformation of ferrous sulfate and copper sulfate solutions in the presence of sodium hydroxide into copper iron hydroxide ($Cu(OH)_2{\cdot}2Fe(OH)_2$) precursors. The formed precursors were then converted to copper ferrite by thermal treatment at different hydrothermal temperatures according to the following equations:

$$Fe^{2+} + SO_4^{2-} \rightarrow FeSO_4 \quad (4)$$

$$Cu^{2+} + H_2SO_4 \rightarrow CuSO_4 + 2H^+ \quad (5)$$

$$2FeSO_4 + CuSO_4 + 6NaOH \rightarrow Cu(OH)_2 \cdot 2Fe(OH)_2 + 3Na_2SO_4 \quad (6)$$

$$Cu(OH)_2 \cdot 2Fe(OH)_2 + 1/2O_2 \rightarrow CuFe_2O_4 + 3H_2O \quad (7)$$

Fig. 3a shows XRD patterns of the produced copper ferrites samples at different variables of different hydrothermal temperatures, hydrothermal times and pH values. From Table 2 and Fig. 3a, the results showed that at low hydrothermal temperatures 100 °C, low hydrothermal time 12 h and pH 10, Three phases were formed; cubic copper ferrite, c-$CuFe_2O_4$ (JCPDS # 77-10), hematite, Fe_2O_3, (JCPDS # 89-0596) and copper(I) oxide, Cu_2O (JCPDS # 77-0199) phases (R1). By increasing hydrothermal time to (36 h) at same

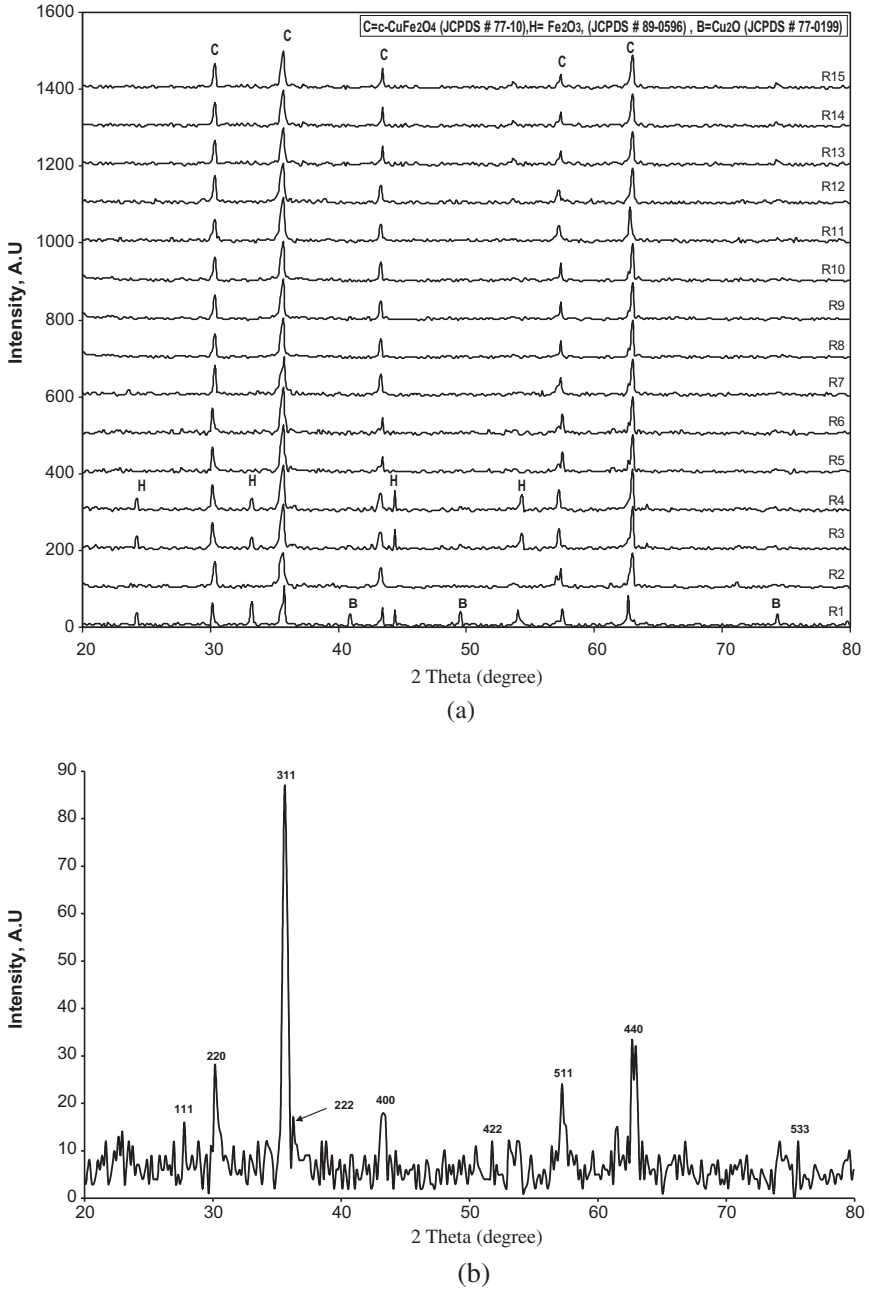

Fig. 3. XRD analysis of the produced copper ferrite powders (a) all 15 experiments and (b) R5 sample at 100 °C, 24 h and pH 8.

Table 2
Experimental Box–Behnken design (hydrothermal temperatures 100–200 °C, hydrothermal times 12–36 h and pH values 8–12) on phase formation, crystallite size and magnetic properties.

R. No	Factors			Response				Phases
	Temperature (°C)	Time (h)	pH	M_s (emu/g)	M_r (emu/g)	H_c (Oe)	CS (nm)	
1	100	12	10	37.31	1.41	125.8	51.5	c-$CuFe_2O_4$, Fe_2O_3, Cu_2O
2	200	12	10	79.98	0.53	121.7	39.6	c-$CuFe_2O_4$
3	100	36	10	42.74	1.46	125.3	45.4	c-$CuFe_2O_4$, Fe_2O_3
4	200	36	10	59.77	1.91	138.7	42.1	c-$CuFe_2O_4$, Fe_2O_3
5	100	24	8	69.05	0.75	80.26	26.2	c-$CuFe_2O_4$
6	200	24	8	83.7	3.95	72.14	32.5	c-$CuFe_2O_4$
7	100	24	12	74.08	4.50	90.32	30.5	c-$CuFe_2O_4$
8	200	24	12	70.02	3.20	102.1	29.2	c-$CuFe_2O_4$
9	150	12	8	68.02	2.98	62.48	29.9	c-$CuFe_2O_4$
10	150	36	8	73.29	3.39	83.25	26.5	c-$CuFe_2O_4$
11	150	12	12	68.25	2.15	79.47	24.6	c-$CuFe_2O_4$
12	150	36	12	74.52	4.37	75.11	32.8	c-$CuFe_2O_4$
13	150	24	10	68.58	3.76	107.1	37.8	c-$CuFe_2O_4$
14	150	24	10	65.92	3.94	108.2	36.0	c-$CuFe_2O_4$
15	150	24	10	71.55	4.4	117	35.1	c-$CuFe_2O_4$

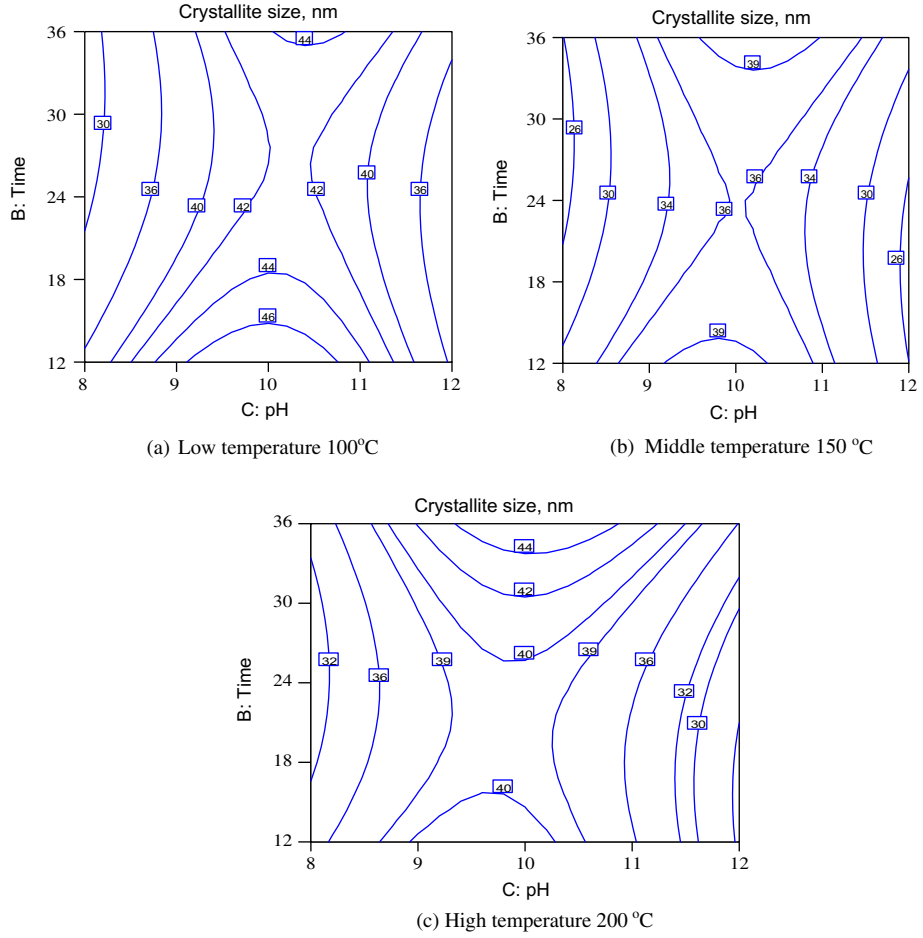

(a) Low temperature 100°C (b) Middle temperature 150 °C

(c) High temperature 200 °C

Fig. 4. Contour plots for the effect of reaction time (h) and pH on the copper ferrite crystallite size at different temperatures (100, 150 and 200 °C).

previous conditions, two phase's c-$CuFe_2O_4$ as a major phase and hematite Fe_2O_3 as a minor phase were obtained (R3). At all remains experimental conditions, a pure well crystalline single phase of cubic copper ferrite was obtained (R 2, 5, 6, 7, 8, 9, 10, 11, 12, 13, 14 and 15) with different crystallite size of $CuFe_2O_4$ nanopowders. The average crystallite size was decreased by increasing the temperature. It decreased from 51.5 nm at low hydrothermal temperature 100 °C to 39.6 nm at high hydrothermal temperature 200 °C (R1 and R2). This can be explained in terms of formation of pure high well crystalline phase of cubic $CuFe_2O_4$ phase without other phases. At R_3 and R_4, The crystallite size was decreased from 45.4 nm at low hydrothermal temperature 100 °C to 42.1 nm at high hydrothermal temperature 200 °C. At low pH value 8, the crystallite size was increased by increasing the temperature. It increased from 26.25 nm at low hydrothermal temperature 100 °C to 32.5 nm at high hydrothermal temperature 200 °C. This is

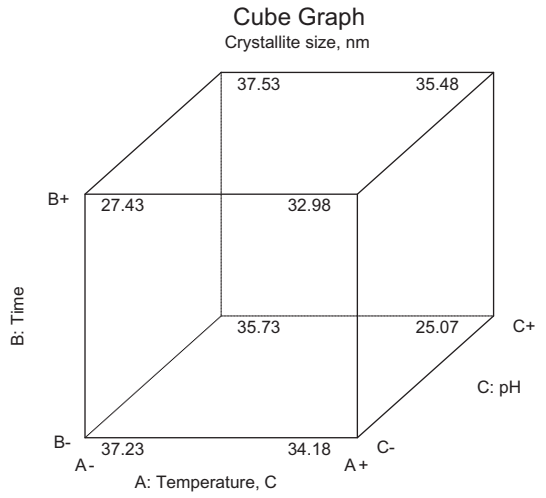

Fig. 5. D plots for all experimental data [(time (h), temperature (°C) and pH] on the crystallite size of the cubic copper ferrite powders.

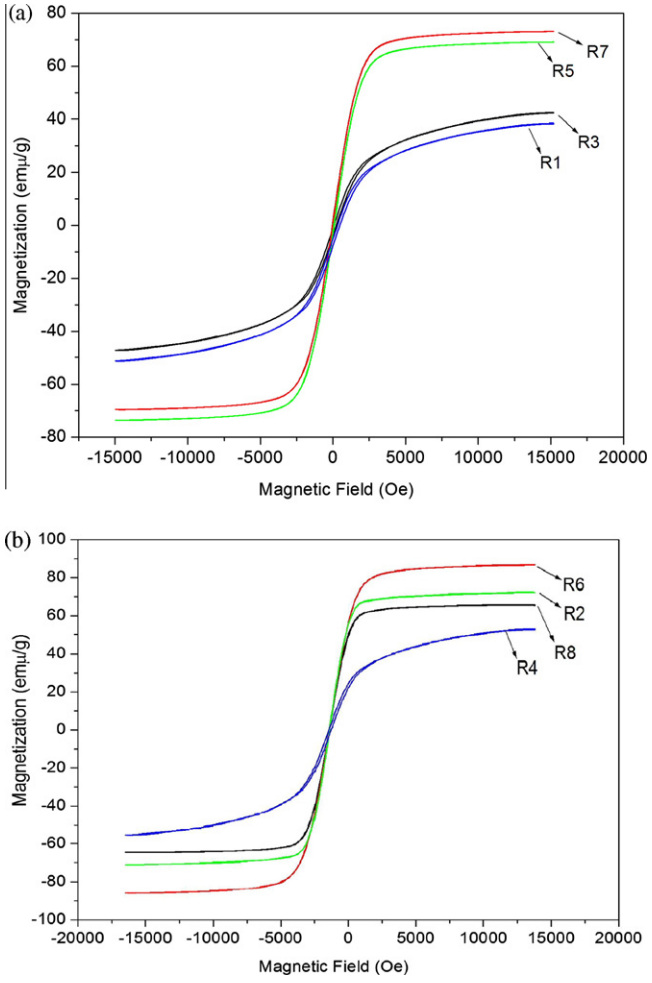

Fig. 6. *M–H* hysteresis loop of the produced cubic copper ferrite powders: (a) hydrothermally treated at 100 °C and (b) hydrothermally treated at 200 °C.

explained in terms of agglomeration of the particles together which lead to larger crystallite size**.** XRD pattern of the produced copper ferrite nanopowders by hydrothermal method showed the presence of pure single phase of cubic copper ferrite as shown in Fig. 3b. The diffraction patterns were related to the cubic copper ferrite phase (JCPDS # 77-10).

Statistical design showed the change of the crystallite size of copper ferrite phase at different synthesis conditions using hydrothermal method. The standard deviation was 3.57 and, the determination coefficient *R*-square 0.9213 which indicated the agreement of the generated model and the experimental results. It is observed that the average crystallite size of produced copper ferrite powders at all experiments ranged from 24.6 nm to 51.5 nm.

The effects of hydrothermal time and pH at different hydrothermal temperatures from 100 to 200 °C on the crystallite size of the produced copper ferrite nanoparticles were studied in the basis of contour plots produced from Box–Behnken statistical design program and the results are given in Fig. 4. It was clear that at low temperature, the hydroxyl-complex, $Cu(OH)_2{\cdot}2Fe(OH)_3$, had no sufficient activated diffusion migration energy at such temperature, 100 °C, and crystallization process became very slow to form small nanosize particle. With the temperature raising the activated diffusion migration energy was enough to form $CuFe_2O_4$ with crystallite size 26 nm. As the temperature reached 200 °C, crystallite size was increased again and this may be explained on the basis of the agglomeration of the particle.

Similar way for low, middle and high temperature was observed where, through all the time range, increasing pH to 10 the crystallite size was increased and further pH increasing crystallite size was decreased.

All the experimental data, collected at the 3-D cubic graph as shown in Fig. 5 revealed the lowest crystallite size (25.07 nm) can be obtained at high levels of both hydrothermal temperature and pH and low level of hydrothermal time. The highest crystallite size (37.53 nm) can be obtained at high levels of hydrothermal time and pH and low level of hydrothermal temperature. The optimum lowest crystallite size (24.6 nm) was obtained at hydrothermal temperature 150 °C, hydrothermal time 12 h and pH 12. The highest crystallite size (51.5 nm) was obtained at hydrothermal temperature 100 °C, time 12 h and pH 10.

The magnetization of the produced $CuFe_2O_4$ powders using vibrating sample magnetometer was performed at room temperature under an applied field of 15 kOe and the hysteresis loops of the ferrite powders were obtained. Plots the magnetization *M* as a function of applied field *H* per hydrothermal temperature, hydrothermal time and pH were shown in Fig. 5 and the magnetic parameters were summarized in Table 2. From Fig. 6 and Table 2, the results illustrated that high saturation magnetization (83.7 emu/g) can be achieved at high hydrothermal temperature 200 °C with middle time 24 h and low pH value 8 (sample R6) whereas high coercive force (138.7 Oe) can be achieved at high levels of temperature 200 °C and time 12 h, and middle pH 10 for the sample R4. The high value of saturation magnetization was attributed to the formation of well crystalline single phase of cubic-copper ferrite phase with high crystallinity and well crystallite size whereas the high coercive force can be attributed to the presence of hematite impurity Fe_2O_3 phase with the produced copper ferrite. Moreover, the variation of H_c with crystallite size can be explained on the basis of domain structure, critical diameter and the anisotropy of the crystal. A crystallite will spontaneously break up into a number of domains in order to reduce the large magnetization energy it would have if it were a single domain [33]. Lower saturation magnetization (37.3 emu/g) was attributed to the formation of nonmagnetic impurities phases of copper and iron oxides.

Fig. 7 showed the effect of hydrothermal time and pH on saturation magnetization of copper ferrite powders at different hydrothermal temperatures. The statistical design showed that the standard deviation was 7.73 and R^2 was 0.8060 that described our results make sense. No interaction between any two synthesis parameters was found using the statistical design data.

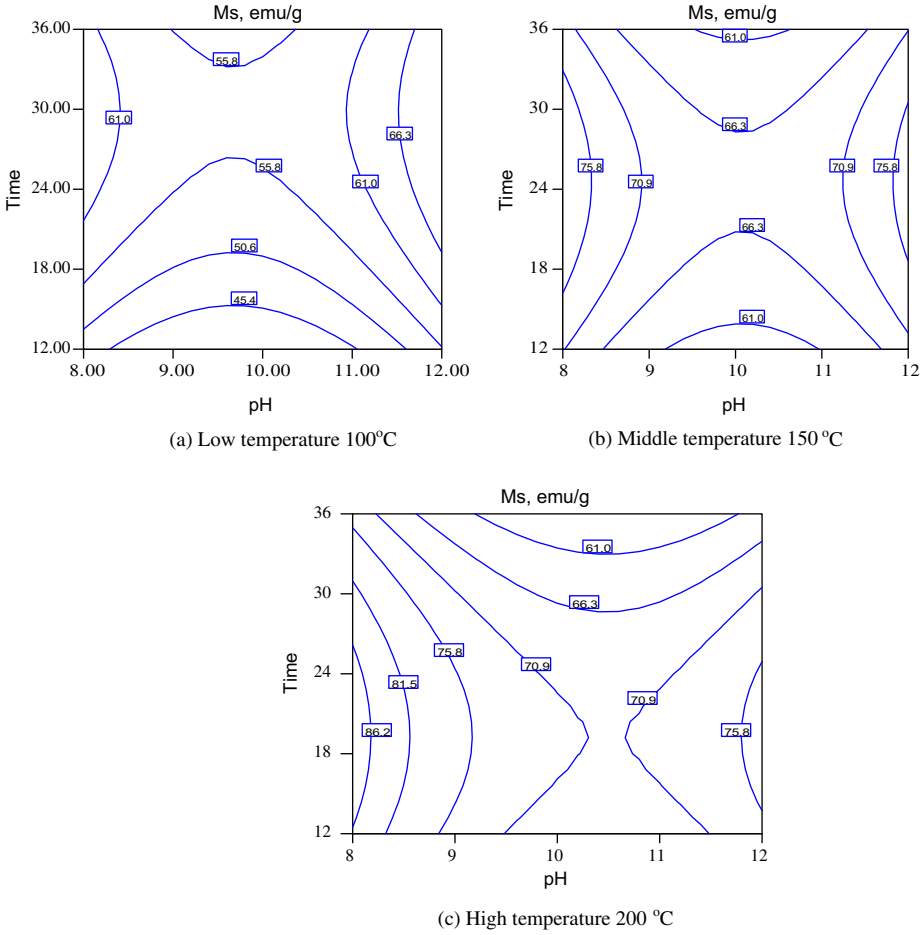

(a) Low temperature 100°C (b) Middle temperature 150 °C

(c) High temperature 200 °C

Fig. 7. Contour plots for the effect of reaction time (h) and pH on the saturation magnetization of copper ferrite powders at different temperatures (100, 150 and 200 °C).

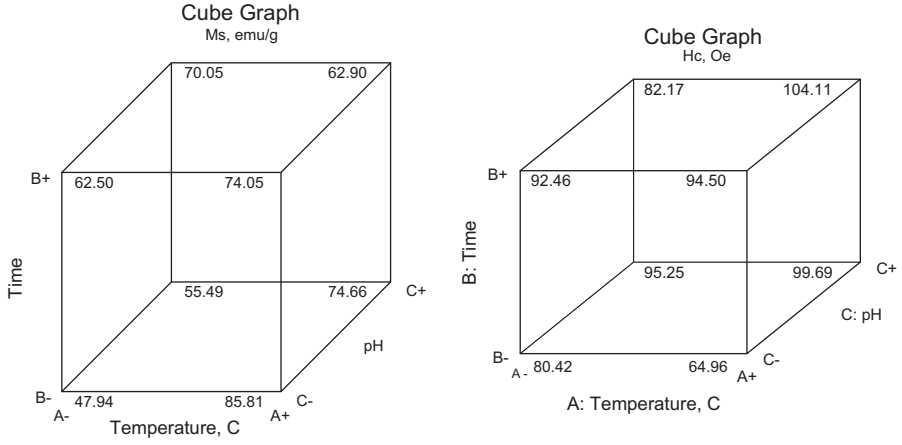

(a) (b)

Fig. 8. D plots for all experimental data [(time (h), temperature (°C) and pH on (a) saturation magnetization M_s and (b) Coercive force H_c of the produced cubic copper ferrite powders.

At low temperature, the increasing of time led to increasing the saturation magnetization. Furthermore, at middle pH 9.5–10.3, the saturation magnetization was increased by increasing the hydrothermal time. At middle temperature level 150 °C, the saturation magnetization was increased compared with low temperature level 150 °C. Furthermore, the saturation magnetization was increased by increasing the hydrothermal time at middle pH level. The highest saturation magnetization (M_s = 86.2 emu/g) can be achieved at high level of hydrothermal temperature 200 °C, low pH 8 and middle level of hydrothermal time 26 h. Increasing the pH level with increasing the hydrothermal time led to decrease in saturation magnetization which can be attributed to the

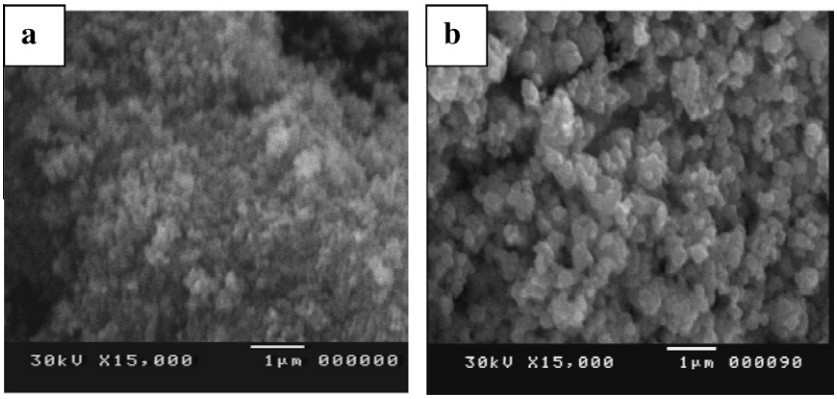

Fig. 9. SEM micrographs of the produced copper ferrite: (a) hydrothermal temperature 150 °C, hydrothermal time 12 h and pH 8 (R9 sample) and (b) hydrothermal temperature 200 °C, hydrothermal time 24 h, and pH 12 (R8 sample).

Table 3
Photocatalyic degradation of methylene blue using cubic copper ferrite powders.

Run No.	Temperature (°C)	Time (h)	pH	CS (nm)	S_{BET} (m^2/g)	Phases	Degradation (%)
R_2	200	12	10	39.6	95.2	c-$CuFe_2O_4$	88.8
R_4	200	36	10	42.1	56.9	c-$CuFe_2O_4$, Fe_2O_3	80.0
R_8	200	24	12	29.2	118.4	c-$CuFe_2O_4$	95.9
R_9	150	12	8	29.9	89.7	c-$CuFe_2O_4$	87.8
R_{10}	150	36	8	26.5	108.3	c-$CuFe_2O_4$	93.9

possibility of dissociation of the formed copper ferrite powders to form secondary phases of CuO and Fe_2O_3.

All the experimental results, collected at the 3-D cubic graph as shown in Fig. 8a revealed that saturation magnetization (M_s), which ranged from 47.94 to 85.81 emu/g, could be produced. The highest saturation magnetization (M_s = 85.81 emu/g) can be achieved at high level of temperature and low levels of both time and pH. On the other hand, the smallest saturation magnetization (M_s = 47.94 emu/g) can be obtained at low levels of temperature, time and pH. The experimental optimum high saturation magnetization 83.7 emu/g was achieved at high hydrothermal temperature 200 °C with middle time 24 h and low pH value 8 whereas the lowest saturation magnetization (37.5 emu/g) was obtained at low temperature 100 °C, low hydrothermal time 12 h and middle pH 10. On the other hand, 3-D cubic graph as shown in Fig. 8b indicated that H_c, which ranged from 64.96 to 104.11 Oe could be produced. The highest coercivity (H_c value 104.11 Oe) can be achieved at high levels of temperature, time and pH. The highest value is lower than the experimental data which explained the deviation of statistical design model than the experimental data. On the other hand, the smallest coercivity (H_c value 64.96 Oe) can be obtained at high level of temperature and low levels of both time and pH. In comparison with the experimental results, A high coercive field H_c (138.7 Oe) was attained at high hydrothermal temperature 200 °C, high time 36 h and middle pH 10 whereas a low coercive field H_c (62.5 Oe) was formed at middle hydrothermal temperature 150 °C, low time 12 h and low pH 8.

The scanning electron microscopy (SEM) micrographs for copper ferrite obtained at hydrothermal temperature 150 °C, hydrothermal time 12 h and pH 8 showed that very fine and homogenous nanospheres copper ferrite particles contained some agglomeration. The agglomeration of particles was related to many factors such as shape factor, surface area, porosity, and density. Moreover, most colloidal particles are electrically charged, e.g., most metal oxides have a surface layer of the metal hydroxide which is amphoteric and can become either positively or negatively charged, by taking up a proton or by proton abstraction, depending on the pH. The electrostatic potential on the particle surface, relative to the surrounding fluid, is strongly dependent on the balance between the positive and negative ions. For the oxide systems, and many other colloids, the H^+ and OH^- ions are the potential-determining ions. In such systems, the surface charge and potential are determined largely by the balance between H^+ and OH^- in solution, i.e., by the pH [34]. The particles were close to each other in a regular and a uniform manner to form the spherical-like structure (Fig. 9a). Increasing the synthesis conditions of the produced cooper ferrite at hydrothermal temperature 200 °C, hydrothermal time 24 h, and pH 12 modified the microstructure to the pseudo-cubic-like structure with a high uniform grain structure (Fig. 9b).

Table 3 shows the photocatalytic degradation of methylene blue by copper ferrite photo catalyst. The results showed that the crystallite size and the phase formed were the main factors for photodegradation of methylene blue. Maximum photodegradation (95.9%) can be attained at crystallite size 29.2 nm. Minimum photodegradation (80.0%) can be attained at crystallite size 42.1 nm. Furthermore, although the crystallite size of the sample R9 is slightly similar to R8, the Photocatalytic degradation was decreased from 95.9% to 87.8%. This may be due to the decrease in the surface area of the sample as shown in Table 3. The results can be explained in basis of the decrease in crystallite size increases the surface area and thereby increases available average active sites. Decrease in crystallite size also increases higher photo-ionic efficiency from a higher interfacial charge carrier transfer rate. This shows that the photodecomposition activity for MB is higher for smaller crystallite size of pure copper ferrite. Highest photoactivity seems to be reasonable because this sample contains the highest c-$CuFe_2O_4$ crystallinity and the significant decrease in the photocatalytic activity of $CuFe_2O_4$ might be attributed to the variation in phase composition and in particle size in addition to more uniform size of $CuFe_2O_4$ particles with lower aggregation of crystallites The significant increase in the photodecomposition rate seems to be related to electrons scavenging, R^+, as well as production of additional oxidizing species, ·OH, hydroxyl radical [35,36].

4. Conclusions

The results can be summarized as follows:

– Cubic copper ferrite nanoparticles have been synthesized via hydrothermal method at different temperatures from 100 to 200 °C for times from 12 to 36 h with pH values 8–12.

- The synthesis conditions have strongly influenced on the crystal structure, crystallite size, microstructure, magnetic and photocatalytic properties.
- The crystallite size of the produced copper ferrite powders was in the range between 24.6 and 51.5 nm.
- The lowest crystallite size (24.6 nm) was obtained at hydrothermal temperature 150 °C, hydrothermal time 12 h and pH 12. The highest crystallite size (51.5 nm) was obtained at hydrothermal temperature 100 °C, time 12 h and pH 10.
- High saturation magnetization 83.7 emu/g was achieved at high hydrothermal temperature 200 °C with middle time 24 h and low pH value 8 due to well pure crystalline cubic copper ferrite phase formed, whereas high coercive force 138.7 Oe can be achieved at low levels of temperature 100 °C and time 12 h, and middle pH 10 due to formation of α-Fe_2O_3 with $CuFe_2O_4$ phase.
- The microstructures of the produced powders were affected with the synthesis conditions. The particles appeared as nanospheres at hydrothermal temperature 150 °C, hydrothermal time 12 h and pH 8 which changed to the pseudo-cubic-like structure at hydrothermal temperature 200 °C, hydrothermal time 12 h and pH 8.
- Photocatalytic degradation of the methylene blue dye from aqueous solution was studied. So the produced cubic copper ferrite powders from the industrial wastes were used as W/W (waste for treatment of other waste). The catalytic efficiency was 95.9% at hydrothermal temperature 200 °C for hydrothermal time 24 h at pH 12 due to high surface area 118.4 m^2/g.

References

[1] S.D. Sartale, C.D. Lokhande, M. Muller, Electrochemical synthesis of nanocrystalline $CuFe_2O_4$ thin films from non-aqueous (ethylene glycol) medium, Mater. Chem. Phys. 80 (2003) 120–128.

[2] Z. Sun, L. Liu, D.z. Jia, W. Pan, Simple synthesis of $CuFe_2O_4$ nanoparticles as gas-sensing materials, Sens. Actuators, B: Chem. 125 (2007) 144–148.

[3] K.-S. Kang, C.-H. Kim, W.-C. Cho, K.-K. Bae, S.-W. Woo, C.-S. Park, Reduction characteristics of $CuFe_2O_4$ and Fe_3O_4 by methane; $CuFe_2O_4$ as an oxidant for two-step thermochemical methane reforming, Int. J. Hydrogen Energy 33 (2008) 4560–4568.

[4] S. Kameoka, T. Tanabe, A.P. Tsai, Self-assembled porous nano-composite with high catalytic performance by reduction of tetragonal spinel $CuFe_2O$, Appl. Catal., A: Gen. 375 (2010) 163–171.

[5] N. Nasrallah, M. Kebir, Z. Koudri, M. Trari, Photocatalytic reduction of Cr(VI) on the novel hetero-system $CuFe_2O_4$/CdS, J. Hazard. Mater. 185 (2011) 1398–1404.

[6] R.K. Selvan, N. Kalaiselvi, C.O. Augustin, C.H. Doh, C. Sanjeeviraja, $CuFe_2O_4$/SnO_2 nanocomposites as anodes for Li-ion batteries, J. Power Sources 157 (2006) 522–527.

[7] S. Roy, J. Ghose, Mössbauer study of nanocrystalline cubic $CuFe_2O_4$ synthesized by precipitation in polymer matrix, J. Magn. Magn. Mater. 307 (2006) 32–37.

[8] R.K. Selvan, C.O. Augustin, L.J. Berchmans, R. Saraswathi, Combustion synthesis of $CuFe_2O_4$, Mater. Res. Bull. 38 (2003) 41–54.

[9] M. Sultan, R. Singh, Magnetization and crystal structure of RF-sputtered nanocrystalline $CuFe_2O_4$ thin films, Mater. Lett. 63 (2009) 1764–1766.

[10] W. Ponhan, S. Maensiri, Fabrication and magnetic properties of electrospun copper ferrite ($CuFe_2O_4$) nanofibers, Solid State Sci. 11 (2009) 479–484.

[11] J.E. Tasca, C.E. Quincoces, A. Lavat, A.M. Alvarez, M.G. González, Preparation and characterization of $CuFe_2O_4$ bulk catalysts, Ceram. Int. 37 (2011) 803–812.

[12] E. Manova, T. Tsoncheva, D. Paneva, M. Popova, N. Velinov, B. Kunev, K. Tenchev, I. Mitov, Nanosized copper ferrite materials: mechanochemical synthesis and characterization, J. Solid State Chem., in press, doi:10.1016/J.JSSC.2011.03.035.

[13] S. Bassaid, M. Chaib, S. Omeiri, A. Bouguelia, M. Trari, Photocatalytic reduction of cadmium over $CuFeO_2O_4$ synthesized by sol gel, J. Photochem. Photobiol., A: Chem. 201 (2009) 62–68.

[14] T. Tsoncheva, E. Manova, N. Velinov, D. Paneva, M. Popova, B. Kunev, K. Tenchev, I. Mitov, Thermally synthesized nanosized copper ferrites as catalysts for environment protection, Catal. Commun. 12 (2010) 105–109.

[15] T. Liu, L. Wang, P. Yang, B. Hu, Preparation of nanometer $CuFe_2O_4$ by auto-combustion and its catalytic activity on the thermal decomposition of ammonium perchlorate, Mater. Lett. 62 (2008) 4056–4058.

[16] T.G. Altincekic, İ. Boz, A. Baykal, S. Kazan, R. Topkaya, M.S. Toprak, Synthesis and characterization of $CuFe_2O_4$ nanorods synthesized by polyol route, J. Alloys Compd. 493 (2010) 493–498.

[17] J. Du, Z. Liu, W. Wu, Z. Li, B. Han, Y. Huang, Preparation of single-crystal copper ferrite nanorods and nanodisks, Mater. Res. Bull. 40 (2005) 928–935.

[18] H.-C. Lu, J.-E. Chang, P.-H. Shih, L.-C. Chiang, Stabilization of copper sludge by high temperature $CuFe_2O_4$ synthesis process, J. Hazard. Mater 150 (2008) 504–509.

[19] B. Tang, L. Yuan, T. Shi, L. Yu, Y. Zhu, Preparation of nano-sized magnetic particles from spent pickling liquors by ultrasonic-assisted chemical co-precipitation, J. Hazard. Mater. 163 (2009) 1173–1178.

[20] J. Yang, J. Peng, K. Liu, R. Guo, D. Xu, J. Jia, Synthesis of ferrites obtained from heavy metal solutions using wet method, J. Hazard. Mater. 143 (2007) 379–385.

[21] J. Yang, J. Peng, R. Guo, K. Liu, J. Jia, D. Xu, Optimization and thermodynamic assessment of ferrite (Fe_3O_4) synthesis in simulated wastewater, J. Hazard. Mater. 149 (2007) 106–114.

[22] J. Nan, D. Han, M. Cui, M. Yang, L. Pan, Recycling spent zinc manganese dioxide batteries through synthesizing Zn–Mn ferrite magnetic materials, J. Hazard. Mater. 133 (2006) 257–261.

[23] Y.M.Z. Ahmed, M.M. Hessien, M.M. Rashad, Nano-crystalline copper ferrites from secondary iron oxide (mill scale), J. Magn. Magn. Mater. 321 (2009) 181–187.

[24] M.M. Rashad, M.H. Khedr, K.S. Abdel-Halim, Magnetic and catalytic properties of $Cu_{0.5}Zn_{0.5}Fe_2O_4$ nanocrystallite powders, J. Nanosci. Nanotechnol. 6 (2006) 114–119.

[25] M.M. Rashad, O.A. Fouad, Synthesis and characterization of nano-sized nickel ferrites from fly ash for catalytic oxidation of CO, Mater. Chem. Phys. 94 (2005) 365–370.

[26] M.M. Rashad, H. El-Shall, Effect of synthesis conditions on the preparation of $MgSnO_3$ powder via co-precipitation method, Powder Technol. 183 (2008) 161–168.

[27] E.A. Abdel-Aal, S.M. Malekzadeh, M.M. Rashad, A.A. El-Midany, H. El-Shall, Effect of synthesis conditions on preparation of nickel metal nanopowders via hydrothermal reduction technique, Powder Technol. 171 (2007) 63–68.

[28] M.M. Rashad, R.S. Mohamed, A.A. El-Midany, A.T. Kandil, I.A. Ibrahim, Application of statistical design to optimize the preparation of barium titanate nanopowders via oxalate precursor method, Eurasian Chem. Technol. J. 9 (2) (2007) 113–119.

[29] M.M. Rashad, M.M. Hessien, A. El-Midany, I.A. Ibrahim, Effect of synthesis conditions on the preparation of YIG powders via co-precipitation method, J. Magn. Magn. Mater. 321 (2009) 3752–3757.

[30] M.M. Rashad, M.M. Hessien, E.A. Abdel-Aal, K. El-Barawy, R.K. Singh, Transformation of silica fume into chemical mechanical polishing (CMP) nano-slurries for advanced semiconductor manufacturing, Powder Technol. 205 (2011) 149–154.

[31] M. Raffin, E. Germain, S. Judd, Optimising operation of an integrated membrane system (IMS) – a Box–Behnken approach, Desalination 273 (2011) 136–141.

[32] S. Raffellini, M. Schenk, S. Guerrero, S.M. Alzamora, Kinetics of *Escherichia coli* inactivation employing hydrogen peroxide at varying temperatures, pH and concentrations, Food Control 22 (2011) 920–932.

[33] M.A. Gabal, Structural and magnetic properties of nano-sized Cu–Cr ferrites prepared through a simple method using egg white, Mater. Lett. 64 (2010) 1887–1890.

[34] M.M. Rashad, Z.I. Zaki, H. El-Shall, A novel approach for synthesis of nanocrystalline $MgAl_2O_4$ powders by co-precipitation method, J. Mater. Sci. 44 (2009) 2992–2998.

[35] V. Ramaswamy, B. Jagtap, S. Vijayanand, S. Bhange, P. Awati, Photocatalytic decomposition of methylene blue on nanocrystalline titania prepared by different methods, Mater. Res. Bull. 43 (2008) 1145–1152.

[36] A. Syoufian, K. Nakashima, Degradation of methylene blue in aqueous dispersion of hollow titania photocatalyst: optimization of reaction by peroxydisulfate electron scavenger, J. Colloid Interface Sci. 313 (2007) 213–218.